Hydrology Research

Hydrology Research Vol 55 No 3, 392 doi: 10.2166/nh.2024.185

Revealing temporal variation of baseflow and its underlying causes in the source region of the Yangtze River (China)

Guangdong Wu [a], Jianyun Zhang [b,*], Yunliang Li [c], Yanli Liu [b], Huazhun Ren [d] and Mingzhi Yang [a]

[a] Changjiang River Scientific Research Institute, 23 Huangpu Road, Wuhan 430010, China
[b] Nanjing Hydraulic Research Institute, 223 Guangzhou Road, Nanjing 210029, China
[c] Nanjing Institute of Geography and Limnology, Chinese Academy of Sciences, 73 East Beijing Road, Nanjing 210008, China
[d] Changjiang Water Resources Commission of the Ministry of Water Resources, 1863 Jiefang Road, Wuhan 430010, China
*Corresponding author. E-mail: jyzhang@nhri.cn

GW, 0009-0007-4863-9056

ABSTRACT

Baseflow plays a crucial role in sustaining the alpine ecosystem during rainless or cold periods. Despite its importance, information on how and why baseflow has changed in the source region of the Yangtze River (SRYR) is sparse. In our study, statistical analysis and the elastic coefficient method were used to identify the dynamic characteristics of baseflow and the underlying causes. The results show that monthly baseflow contributed 62–97% of runoff with a mean value of 75%, and they followed remarkable increasing trends from 1957 to 2020. The contributions of precipitation, temperature, evapotranspiration, and ecological conservation programs (ECPs) on baseflow variations were 86, 53, −15, and −24%, respectively. However, their contributions differed across months. During the warm months of May to September, precipitation played a dominant role, followed by evapotranspiration. In contrast, during other colder months, temperature was dominant; meanwhile, the effect of precipitation was almost absent. Moreover, climatic change had a hysteretic effect on baseflow variation, with a maximum lag time of 10 months. Our results highlighted critical roles of both precipitation and temperature, and indicated that climate change, rather than ECPs, dominated the variation in baseflow in the SRYR.

Key words: baseflow dynamics, climate change, ecological conservation, source region of the Yangtze River

HIGHLIGHTS

- Monthly baseflow contributed 62–97% of runoff with a mean value of 75%.
- Contributions of precipitation, temperature, evapotranspiration, and ecological conservation to the increasing baseflow were 86, 53, −15, and −24%, respectively.
- During warm months, precipitation played a dominant role, while during colder months, the impact of temperature was dominant.
- Climatic change had a hysteretic effect on baseflow variation.

GRAPHICAL ABSTRACT

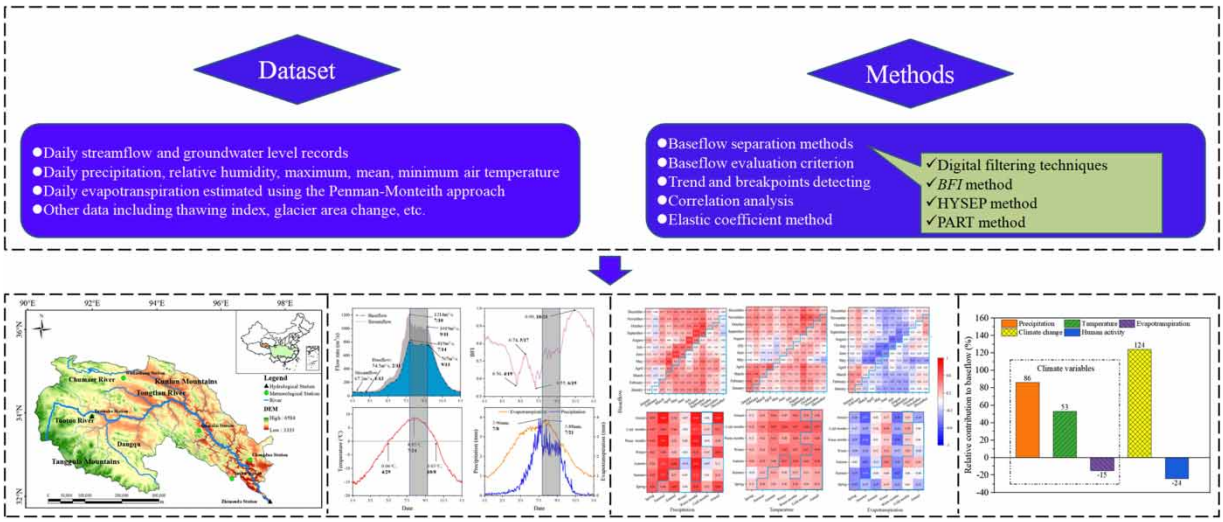

1. INTRODUCTION

The health of river ecosystems is undoubtedly associated with water cycle processes at the basin level (Kayitesi *et al.* 2022). Groundwater flow feeding streams, referred to as baseflow, are an important portion of the watershed hydrologic cycle. Baseflow is the reason many streams do not dry up during dry periods, and it can provide a persistent source of water to streams, sustaining life living in and around them (Guo *et al.* 2022). However, climate variability is expected to intensify or accelerate the hydrologic cycle (Yin *et al.* 2023a, 2023b, 2023c), thereby causing an alteration of the baseflow. At the same time, anthropogenic activity is likely to modify the baseflow regime of watersheds (Chen & Teegavarapu 2021). Prior studies have noted that the baseflow trends of many streams across the globe have experienced profound changes (Ficklin *et al.* 2016). Thus, ensuring sufficient groundwater availability is greatly challenged by climate change and human activities (Scanlon *et al.* 2023). Studying baseflow dynamics and the underlying causes will be important in understanding the evolution of the hydrologic cycle and groundwater storage in changing environments (Brutsaert 2008).

Accurate baseflow estimation is critical for the quantitative management of watershed ecological protection/conservation and the utilization of water resources (Smakhtin 2001). However, few techniques exist to help water managers directly monitor baseflow changes in streams. Numerous baseflow separation approaches have been developed to estimate the baseflow from the streamflow time series. They can be broadly classified into four major categories: hydrograph separation (e.g., HYSEP, flow recession analysis; Ficklin *et al.* 2016; Cheng *et al.* 2017), hydrological model (e.g., SPARROW; Miller *et al.* 2016), numerical simulation (e.g., two-parameter digital filtering method; Eckhardt 2005), and water and chemical mass balance (e.g., geochemical tracers; Tetzlaff & Soulsby 2008). The HYSEP method, as a traditional baseflow segmentation method, is simple but labor-intensive when dealing with long-term series data, and its result is highly subjective (Sloto & Crouse 1996). The physical interpretations of the hydrological model are relatively clear, but its model construction and parameter calibration are complicated and tedious, and the results have a certain degree of uncertainty (Kayitesi *et al.* 2022). The chemical mass balance method separates baseflow by analyzing the composition of stable isotopes in rainfall, surface water, and groundwater, and its results are more reliable. However, it requires large amounts of manpower and material resources and is difficult to widely use (Lott & Stewart 2016). Numerical simulations have been applied worldwide to the baseflow separation of long-term hydrologic series because they are easily operated, efficient, practical, and objective, avoiding the arbitrariness of manual methods (Ahiablame *et al.* 2017). For example, Murray *et al.* (2023) used the Lyne–Hollick one-parameter digital filter method to estimate baseflow and characterized the impacts of climatic change on monthly baseflow trends in Canadian watersheds. However, the baseflow separation results obtained by the above methods may vary, and sometimes the differences are significant. To reduce the uncertainties of the results, it is preferable that multiple baseflow separation methods are adopted simultaneously and qualitatively compared with each other based on their hydrologic plausibility. This serves to select the most suitable method.

With such leaps in understanding the importance of baseflow to stream water dynamics, more research has focused on exploring the factors that control baseflow and how baseflow responds to said factors. In general, the discharge rate of groundwater mainly depends on basin characteristics, climate regime, and human intervention (Segura *et al.* 2019). Watershed characteristics experience minute changes over the course of decades, and as a result, they are largely unnoticeable. Temporal variations of baseflow yield are mainly impacted by climate variability and human intervention (land cover change, increased water utilization, etc.). For example, the reduction of baseflow, which was considered to be the direct reason for the summer drying of the Ganges river, was found to be triggered by groundwater depletion (Mukherjee *et al.* 2018). Groundwater withdrawals were likely accelerating the reduction of baseflow in the heavily irrigated Sao Francisco River basin in Brazil (Lucas *et al.* 2020). Zomlot *et al.* (2015) used the WetSpass water balance model to estimate the recharge rate of 67 hydrologic stations in Flanders, discovering the prominent role of land use changes on recharge variation. Ficklin *et al.* (2016) researched baseflow for 674 sites across the United States, finding that baseflow displayed strong associations with precipitation trends, followed by evapotranspiration. At one point, there was a hypothesis that the baseflow fraction generated by precipitation is primarily attributed to the aridity index, but great differences occurred in humid and arid catchments (Gnann *et al.* 2019). This influence mechanism can be attributed to distinct antecedent wetness. A great many trends in baseflow across Canada were not related to any climatic predictors (Murray *et al.* 2023), likely due to intense anthropogenic activities, such as catchment urbanization, reservoir operation, and river abstractions for industrial, and agricultural, or municipal purposes (Smakhtin 2001). Through summarizing previous studies, we found that many of them were limited to qualitative evaluation about the cause of baseflow change based on correlation analysis. The quantitative attributions of baseflow relative to climate variables and human activities are still rarely discussed, particularly for basins in alpine regions, where temperature plays an important role in driving baseflow variation.

The source region of the Yangtze River (SRYR), located in the hinterland of the Qinghai–Tibet Plateau, is an important part of the Asian Water Tower and China's ecological security barrier. Over the last several decades, the SRYR has suffered unprecedented climate warming and intensified human activities (Cui *et al.* 2023). Consequently, climate change will likely lead to changes in the water cycle processes of the basin, which will then have adverse effects on river ecosystems in the SRYR (Rounce *et al.* 2023). The consistently rising trend in runoff and its related causes have been widely reported (Liu *et al.* 2019; Li *et al.* 2023a, 2023b). However, in-depth studies on the dynamic variations and attributions of baseflow have not been adequately conducted, and the understanding of influence mechanisms in alpine areas remains in the exploratory stage. The primary objectives of this study are to (1) compare the results of multiple baseflow separation methods and select the most appropriate one, (2) clarify the temporal variations of baseflow at various time scales and investigate the associations of baseflow with trends in specific climates, and (3) quantify the relative influences of climate variables (e.g., precipitation, evapotranspiration, temperature) and human activities on baseflow. This study is designed to advance the understanding of baseflow variation and its causes in alpine areas, and to guide future activities regarding water resources management and ecosystem restoration/protection within the SRYR.

2. MATERIALS AND METHODS

2.1. Study area

The SRYR consists of the Tuotuo River (the main source), Dangqu River (the southern source), the Chumaer River (the northern source), and the Tongtian River (the main stream) (Figure 1). The total length of the main stream of the Tongtian River is 1,174 km, with a catchment area of 13.77×10^4 km^2, accounting for 7.6% of total area of the Yangtze River catchments. The source region has an average altitude of 4,500 m above sea level, with the highest point reaching 6,486 m. This area is dominated by unique plateau climates, with an average annual temperature ranging from −17 to −5.5 °C. The precipitation in the area is mainly influenced by warm and humid southwestern air currents and plateau monsoons, with an average annual precipitation ranging from 250 to 600 mm and decreasing from southeast to northwest. Almost 77% of the whole SRYR is covered by a permafrost that spans 107,619 km^2. The seasonally frozen ground covers 30,754 km^2, accounting for 23% of the land, and is primarily distributed in river valleys (Luo 2022). There are more than 300 tributaries, most of which originated from glaciers. SRYR's environments are remote and isolated, with a sparse population, and there are no dams or hydropower stations regulating the flow.

The vegetation that covers the headwaters primarily consists of three types: alpine meadow, grassland, and marsh. Under the joint influences of climate change and anthropogenic disturbance, problems like accelerated permafrost melting,

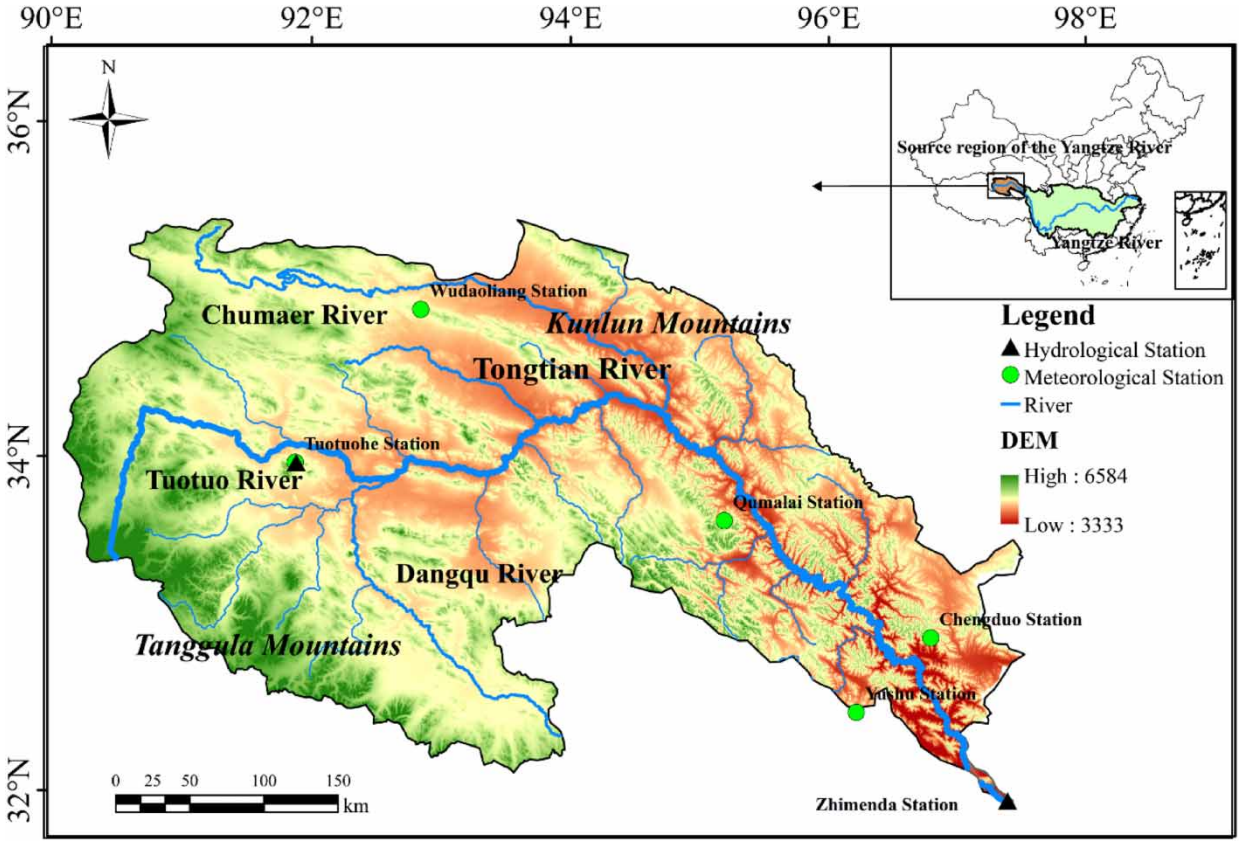

Figure 1 | Location of the source region of the Yangtze River and the distribution of hydrological and meteorological stations.

grassland degradation, soil erosion, and land desertification directly threaten the stability of the rivers' ecosystems and has recently been recognized as a serious social concern (Li *et al.* 2023a, 2023b). Moreover, supra-permafrost water has become a major source of surface water at the Zhimenda and Tuotuohe stations (Li *et al.* 2020), implying that the Yangtze River Water Tower has become increasingly unstable. To prevent further degradation, in 2005, China's State Council invested 7.5 billion yuan RMB to implement more than 22 ecological conservation programs (ECPs) in the Sanjiangyuan Nature Reserve, covering the headwaters of the Yangtze River, the Yellow River, and the Lancang River (Luo 2022).

2.2. Data and source

The SRYR occupies a large area of inaccessible land, so the distribution of hydrological and climate gauges is sparse. Until now, only six hydrological stations have been distributed in the SRYR: the Zhimenda, Tuotuohe, Xinzhai, Yanshiping, Qumalaio, and Longbaotan stations. Unfortunately, all stations, except Zhimenda, have produced patchy observation records. As Zhimenda's hydrometric station is located at the outlet of the SRYR, its daily discharge records were selected for analysis of baseflow characteristics. This station had available data dating back 64 years (1957–2020), and these data were gathered from the Qinghai Hydrological and Water Resources Measurement and Reporting Centre. In addition, we collected meteorological records from five other stations: Tuotuohe, Wudaoliang, Qumalai, Yushu, and Chenduo. These data were provided by the National Meteorological Information Center. These climate data included daily precipitation, relative humidity, and maximum, mean, and minimum air temperatures. The daily potential evapotranspiration data were estimated using the Penman–Monteith approach. The five climate stations mentioned above are representative of the SRYR, and their weighted averages were calculated using the Thiessen polygon. These climate observations provided context for discussing the potential influences of climate change on baseflow. The SRYR topographic map, along with the hydrological and meteorological stations, is presented in Figure 1.

Furthermore, the thawing index was chosen to predict the seasonal ground freeze–thaw and permafrost thaw in the SRYR (Woo *et al.* 2004). The thawing index (°C days) is calculated for each year by summing up the mean daily air temperatures for

all the days exceeding 0 °C (Duan *et al.* 2017). Observed groundwater level records from 2010 to 2020 at the Zhimenda station were selected to reflect groundwater storage variability, and glacier area change data referenced from Li *et al.* (2023a, 2023b) were used to reflect the changes in warming-induced glacier meltwater in the SRYR.

2.3. Baseflow separation approaches

A great many baseflow separation methods have been developed to derive baseflow from the observed streamflow time series. However, applying a single method is risky. Thus, the use of multiple methods to calculate the baseflow is recommended (Tan *et al.* 2020). To obtain accurate estimates of baseflow, seven methods were adopted in our study, including one digital filter method, two baseflow index (BFI) methods, three HYSEP methods, and one PART method. These methods are detailed in the following sections.

2.3.1. Baseflow separation approaches

The recursive digital filtering method originated from a signal processing concept. This process filters the high-frequency signals in the streamflow record associated with surface runoff from the low-frequency signals, which are associated with groundwater discharge or baseflow. Several equation forms were developed to separate the baseflow from the streamflow sequences. The two-parameter digital filtering equation proposed by Eckhardt (2005) is one of the most widely used baseflow separation methods, and thus, was adopted in our study.

$$Q_b(i) = \frac{(1 - \mathrm{BFI}_{\max})\alpha Q_b(i-1) + (1-\alpha)\mathrm{BFI}_{\max} Q(i)}{1 - \alpha \mathrm{BFI}_{\max}} \tag{1}$$

where α is the recession constant and can be obtained from decay analysis. $\mathrm{BFI}_{\max}$ is the maximum BFI, or the maximum ratio of baseflow to total runoff over a long period. $Q(i)$ and $Q_b(i)$ are the total runoff and baseflow at the i time step, respectively.

2.3.2. BFI methods

The BFI procedure was developed by the Institute of Hydrology, Wallingford, United Kingdom, and then programmed by Wahl & Wahl (1995). The BFI method, also known as the minimum sliding method, uses the BFI as a weighing factor to calculate the baseflow. The BFI method mainly includes the standard BFI(f) method and the modified BFI(k) method. Typically, rivers that are recharged by groundwater have a BFI close to 1, while intermittent rivers have a BFI value tending toward 0.

2.3.3. HYSEP methods

The HYSEP software (Sloto & Crouse 1996) uses three methods originally developed by Pettyjohn & Henning (1979) to separate baseflow and runoff components from streamflow hydrographs: the fixed interval method (HYSEP1), the sliding interval method (HYSEP2), and the local minimum method (HYSEP3). These methods use different algorithms to draw connecting lines (baseflow hydrograph) between low points of the streamflow hydrograph. The detailed description of these methods can be seen in Pettyjohn & Henning (1979).

2.3.4. PART methods

The PART method is a procedure proposed by the U.S. Geological Survey for baseflow separation. Baseflow is considered equal to streamflow on days that are designated as being unaffected by surface runoff. The PART method requires daily hydrological series with no less than one hydrologic year. The separation is based on the receding of the antecedent streamflow, which first arranges the daily flow data into a single-dimensional array and then selects the values that meet the recession requirements. If the daily recession has less than a 0.1 log period, the daily streamflow value is used as the baseflow. During the remaining time, the baseflow values are obtained by linear interpolation.

2.4. Baseflow evaluation criterion

Since the applicability of the baseflow separation methods differed in various regions, it was necessary to evaluate their practicalities in the SRYR. Considering that baseflow is relatively stable, the reliability of annual separated baseflow can be assessed using the standard deviation and extreme value ratio of the BFI series. For the purposes of this study, the ratio of annual maximum minus annual minimum to annual minimum was calculated as an extreme value ratio. In addition, strict

baseflow points were selected as baseflow references (considered to be true values). We evaluated the accuracies of seven baseflow separation methods using the Nash–Sutcliffe efficiency (NSE) and Kling–Gupta efficiency (KGE). Strict baseflow points can be obtained using the following four rules: (1) Erase all the data points of daily streamflow with $-dy/dt \geq 0$, where $-dy_i/dt = y_{i+1} - y_{i-1}/2$; (2) Eliminate the previous two points before points with $-dy/dt \geq 0$, as well as the next three points; (3) Eliminate five points after major events that were identified by flood peaks greater than the 90th quantile of all streamflow observations; (4) Exclude data points followed by a data point with smaller dy/dt, namely, $d^2y/dx^2 > 0$ (Xie *et al.* 2020). Detailed explanations of the four rules can be found in Xie *et al.* (2020).

2.5. Trend and breakpoints detecting

The trend in baseflow and its corresponding predictors at annual/seasonal scales from 1957 to 2020 can be estimated using the nonparametric Mann–Kendall test, Sen's Slope test, and linear regression analysis. The Mann–Kendall test was employed to detect whether there are monotonic trends with a significance level of $p = 0.05$ in such long-term time series. The slope of the trend was calculated using Sen's Slope test.

Pettitt's test is widely used for detecting mutations. In our study, Pettitt's test, as well as the Mann–Kendall test, was applied to assess if there were any mutation point in the time series. The results from the two test methods were validated by each other.

2.6. Correlation analyses

The correlation between baseflow and its potential influencing factors was evaluated using the Spearman correlation analysis. The correlation coefficient of two variables (x_i and y_i) is defined as

$$r = \frac{\sum_{i=1}^{n}(x_i - \bar{x})(y_i - \bar{y})}{\sqrt{\sum_{i=1}^{n}(x_i - \bar{x})^2 \sum_{i=1}^{n}(y_i - \bar{y})^2}} \tag{2}$$

The correlation coefficient r ranges from -1 to $+1$. A negative r indicates a negative linear relationship between x and y, and a positive r indicates a positive linear relationship between x and y. The greater the absolute value of r, the stronger the correlation.

2.7. Attribution analysis of baseflow

Numerous methods have been used to quantify the relative contribution of various predictors to hydrological variation. Among them, the elastic coefficient method is popular because of its reliable, cost-effective, and labor-saving advantages in the quantitative estimation of attributions. We used the elasticity approach to quantify the relative contributions of climate factors and human activities to changes in baseflow. The climate elasticity of baseflow is defined as the ratio of the baseflow variation rate to the variation rate of a certain climate factor and is expressed as

$$\varepsilon = \frac{\partial Q_b/Q_b}{\partial X/X} \tag{3}$$

where ε is the climate elasticity of baseflow, Q_b is baseflow, and X indicates precipitation, temperature, or potential evapotranspiration.

Based on the least squares method, the climate elasticity of annual baseflow can be estimated as

$$\varepsilon = \frac{\overline{X}}{\overline{Q_b}} \sum (X_i - \overline{X}) \left(\frac{(Q_{bi} - \overline{Q_b})}{\sum (X_i - \overline{X})^2} \right) = \frac{\rho_{XQ} C_Q}{C_X} \tag{4}$$

where $\overline{Q_b}$ and $\overline{X}$ are multiyear averages of baseflow and climate variables, respectively, C_X and C_Q are variation coefficients in baseflow and climate variables, respectively, and ρ_{XQ} is the correlation coefficient between baseflow and climate variables.

Based on the detected breakpoints, the entire record period can be divided into two sections: the period before the breakpoint is regarded as the baseline period, assumed to be unaffected by human activities, whereas the period after the

breakpoint is considered the change period, assumed to be influenced by human activities; both periods are influenced by climate change. Compared with the baseline period, the climate-induced, precipitation-induced, evapotranspiration-induced, and temperature-induced baseflow variations in the change period were calculated as follows:

$$\Delta\overline{Q}_b^{\text{Climate}} = (\varepsilon_p \Delta P/P + \varepsilon_{PET}\Delta\text{PET}/\text{PET} + \varepsilon_T \Delta T/T)Q_b \tag{5}$$

$$\Delta\overline{Q}_b^{P} = \varepsilon_p Q_b \Delta P/P \tag{6}$$

$$\Delta\overline{Q}_b^{\text{PET}} = \varepsilon_{\text{PET}} Q_b \Delta\text{PET}/\text{PET} \tag{7}$$

$$\Delta\overline{Q}_b^{T} = \varepsilon_T Q_b \Delta T/T \tag{8}$$

where $\Delta\overline{Q}_b^{\text{Climate}}$ indicates the climate-induced change in annual baseflow and ΔP, ΔPET, and ΔT represent changes in precipitation, potential evapotranspiration, and temperature, respectively. Q_b, P, PET, and T are average values of long-term baseflow, precipitation, potential evapotranspiration, and temperature during the baseline period, respectively.

The change in annual baseflow caused by human activities can be calculated as

$$\Delta\overline{Q}_b^{\text{Human}} = \Delta Q_b - \Delta\overline{Q}_b^{\text{Climate}} \tag{9}$$

where ΔQ_b indicates the change in annual baseflow.

Finally, the contribution of climate factors and human activity to baseflow variations can be calculated as follows:

$$P_c = \frac{\Delta\overline{Q}_b^{\text{Climate}}}{|\Delta\overline{Q}_b^{\text{Climate}}| + |\Delta\overline{Q}_b^{\text{Human}}|} \times 100\% \tag{10}$$

$$P_P = \frac{\Delta\overline{Q}_b^{P}}{|\Delta\overline{Q}_b^{\text{Climate}}| + |\Delta\overline{Q}_b^{\text{Human}}|} \times 100\% \tag{11}$$

$$P_{\text{PET}} = \frac{\Delta\overline{Q}_b^{\text{PET}}}{|\Delta\overline{Q}_b^{\text{Climate}}| + |\Delta\overline{Q}_b^{\text{Human}}|} \times 100\% \tag{12}$$

$$P_T = \frac{\Delta\overline{Q}_b^{T}}{|\Delta\overline{Q}_b^{\text{Climate}}| + |\Delta\overline{Q}_b^{\text{Human}}|} \times 100\% \tag{13}$$

$$\text{P}_{\text{Human}} = \frac{\Delta\overline{Q}_b^{\text{Human}}}{|\Delta\overline{Q}_b^{\text{Climate}}| + |\Delta\overline{Q}_b^{\text{Human}}|} \times 100\% \tag{14}$$

3. RESULTS

3.1. Selection of baseflow separation methods

The calculated standard deviation (Figure 2(a)) and the extreme value ratio (Figure 2(b)) showed that the median, mean, and quantile of the BFI sequences from these methods, apart from the PART method, were in the low-value range. The Eckhardt method had the lowest median and mean of the extreme value ratio. It can be inferred that the baseflow derived from the Eckhardt method was the most stable. The results of NSE (Figure 2(c)) and KGE (Figure 2(d)) showed that, among all these baseflow separation methods, the Eckhardt method produced the largest NSE/KGE mean (0.96/0.93) and median (0.97/0.94). It means that the baseflow calculated by the Eckhardt method was closer to the references than that calculated by other methods.

Furthermore, based on hydrologic frequency analysis, the years 1983, 1961, and 1977 were selected as typical high-flow year ($P = 25\%$), moderate-flow year ($P = 50\%$), and low-flow year ($P = 75\%$), respectively. As seen in Figure 3, different hydrological years had similar baseflow hydrographs. For these seven baseflow separation methods, their separation results

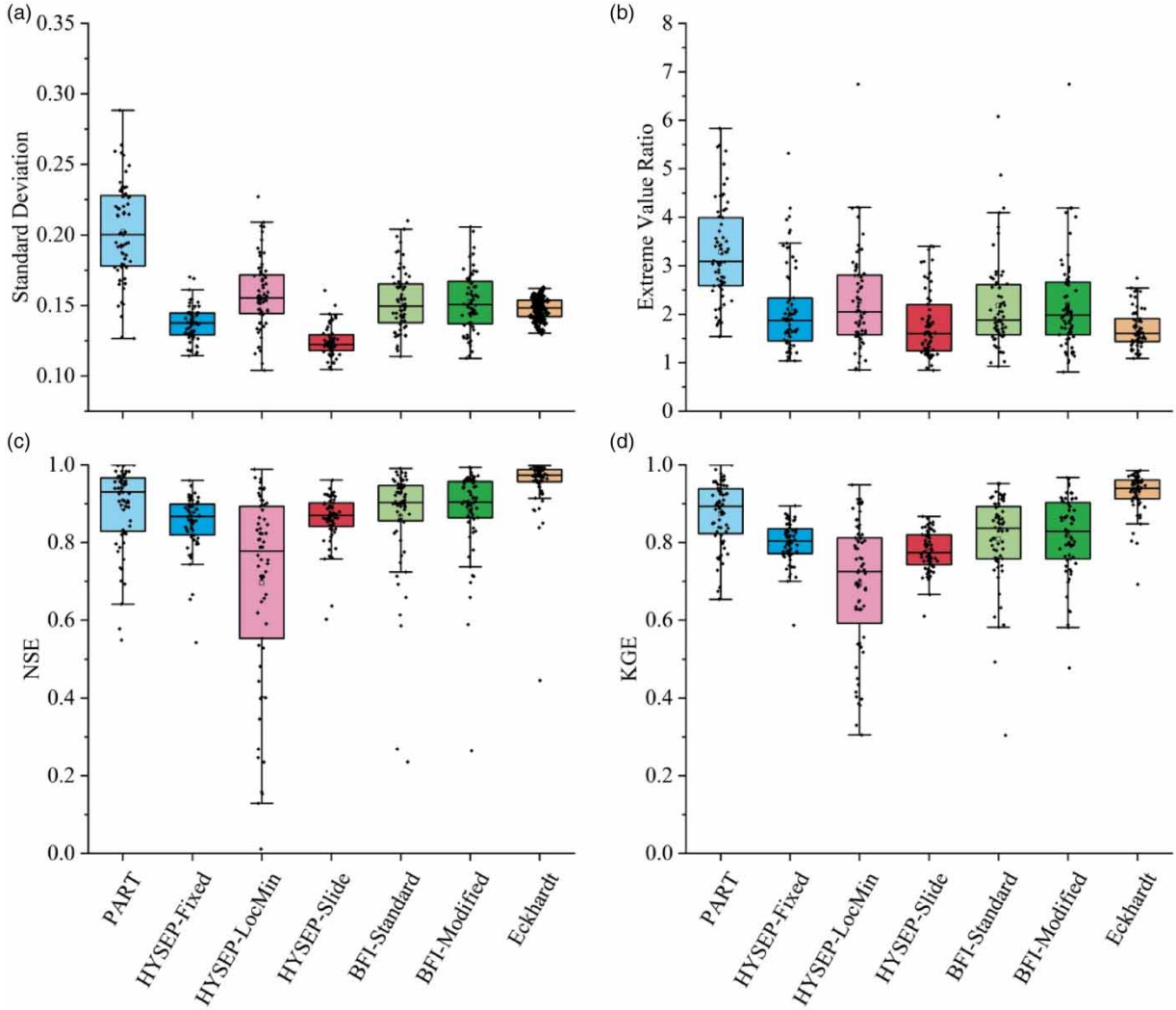

Figure 2 | Box plots of standard deviation (a), extreme value ratio (b) of the annual BFI series, NSE (c), and KGE (d).

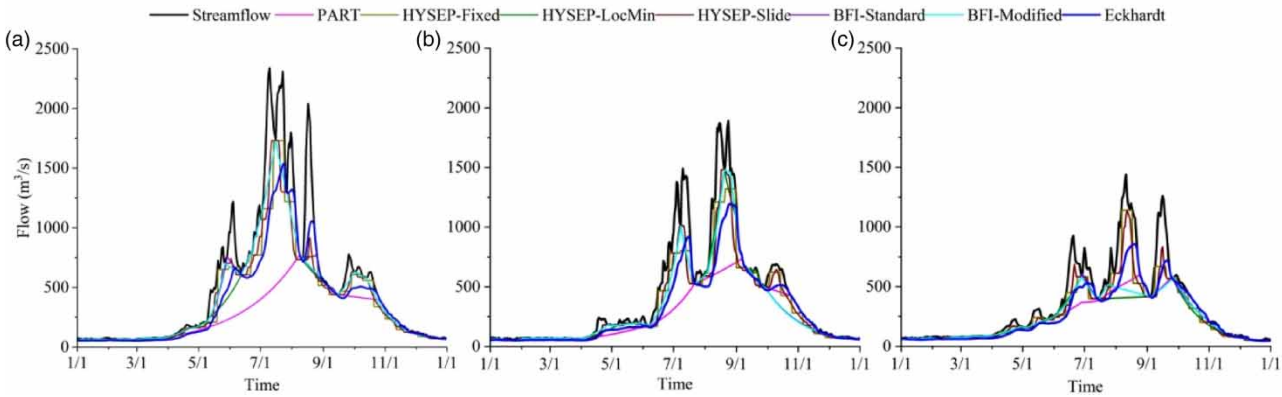

Figure 3 | Hydrographs of streamflow and baseflow during 1983 with high flow (a), 1961 with moderate flow (b), and 1977 with low flow (c).

were similar in dry periods but significantly different in wet periods. For example, the baseflow curves from the HYSEP-Fixed and HYSEP-Slide methods exhibited large fluctuations. Those from the PART, BFI-Standard, BFI-Modified, HYSEP-LocMin, and HYSEP-Slide methods were composed of broken lines, and their lagging behind the streamflow was almost nonexistent. In contrast, the baseflow hydrograph from the Eckhardt method was relatively smooth and presented obvious attenuation and hysteresis effects.

In summary, the Eckhardt method was the most suitable and reliable method for baseflow separation in the SRYR. The upcoming sections will discuss the baseflow and BFI time series derived from the Eckhardt method employed to further analyze the temporal change in baseflow and its potential causes.

3.2. Temporal variability of annual and seasonal baseflow and BFI

Trend analysis results for baseflow and BFI time series from 1957 to 2020 are shown in Table 1 and Figure 4. It was clear that the annual and seasonal baseflow had statistically significant increasing trends, and the significance of baseflow in spring and winter (from December to May of the next year) was greater than that in summer and autumn (from June to November). Despite this, autumn contributed the most to year-round increasing baseflow with a growth rate of 3.04 m^3/s/year, and summer followed closely after, with a growth rate of 2.94 m^3/s/year. Spring and winter contributed the least, with a growth rate of 0.62 and 0.25 m^3/s/year, respectively. In other words, the increasing trend in baseflow in cold months had greater significance than that in warm months. However, the annual increased baseflow volume was attributed to a larger increment of 2.61 m^3/s/year in warm months.

Though the annual BFI, in both warm and cold months, had gradual increasing trends from 1957 to 2020, their trends were not statistically significant. Spring and autumn BFI showed almost no pronounced monotonic trends, while the BFI in summer and winter exhibited statistically insignificant increasing trend. In summary, BFI had a much weaker upward trend compared to baseflow.

The mutation detecting process showed that the abrupt year in annual baseflow was 1998, and those in spring, summer, autumn, and winter were 2004, 1998, 2002, and 2004, respectively. Detecting the temporal pattern in BFI was unsuccessful;

Table 1 | Long-term trend and breakpoints detecting results of annual and seasonal baseflow, BFI, and climate predictors

		Annual	Spring	Summer	Autumn	Winter	Warm months	Cold months
Baseflow	Z	2.80	3.81	2.30	2.51	3.51	2.73	4.22
	Trends	↑	↑	↑	↑	↑	↑	↑
	Trend magnitude in $m^3s^{-1}yr^{-1}$	1.69	0.62	2.94	3.04	0.25	2.61	0.45
	Abrupt point	1998	2004	1998	2002	2004	1998	2004
BFI	Z	1.60	-0.3	0.89	-0.10	1.12	1.43	1.65
	Trends	NS	NS	NS	NS	NS	NS	NS
	Trend magnitude in yr^{-1}	/	/	/	/	/	/	/
	Abrupt point	2000	/	/	/	2006	2000	2006
Precipitation	Z	2.9374	3.7485	1.6048	1.7091	1.1761	2.7983	2.9142
	Trends	↑	↑	NS	NS	NS	↑	↑
	Trend magnitude in mm yr^{-1}	1.14	0.35	0.50	0.25	0.03	1.02	0.10
	Abrupt point	1998	1995	2001	1994	1984	1998	1980
Temperature	Z	6.9002	4.8261	5.4634	5.6488	5.417	6.4947	6.1586
	Trends	↑	↑	↑	↑	↑	↑	↑
	Trend magnitude in ℃ yr^{-1}	0.036976	0.025956	0.028956	0.041508	0.043095	0.02949	0.046467
	Abrupt point	1997	1995	1994	2000	2001	1994	2001
Evapotranspiration	Z	2.2537	0.74738	0.97912	0.9096	3.6094	1.292	3.1807
	Trends	↑	NS	NS	NS	↑	NS	↑
	Trend magnitude in mm yr^{-1}	0.61112	0.10866	0.11814	0.096997	0.29683	0.29735	0.41488
	Abrupt point	1969	1969	1968	1968	2001	1968	2001

Notes: NS = non-significant trend. March to May, June to August, September to November, and December to February were selected to represent spring, summer, fall, and winter, respectively. April to September and October to March were chosen to represent warm and cold months, respectively.

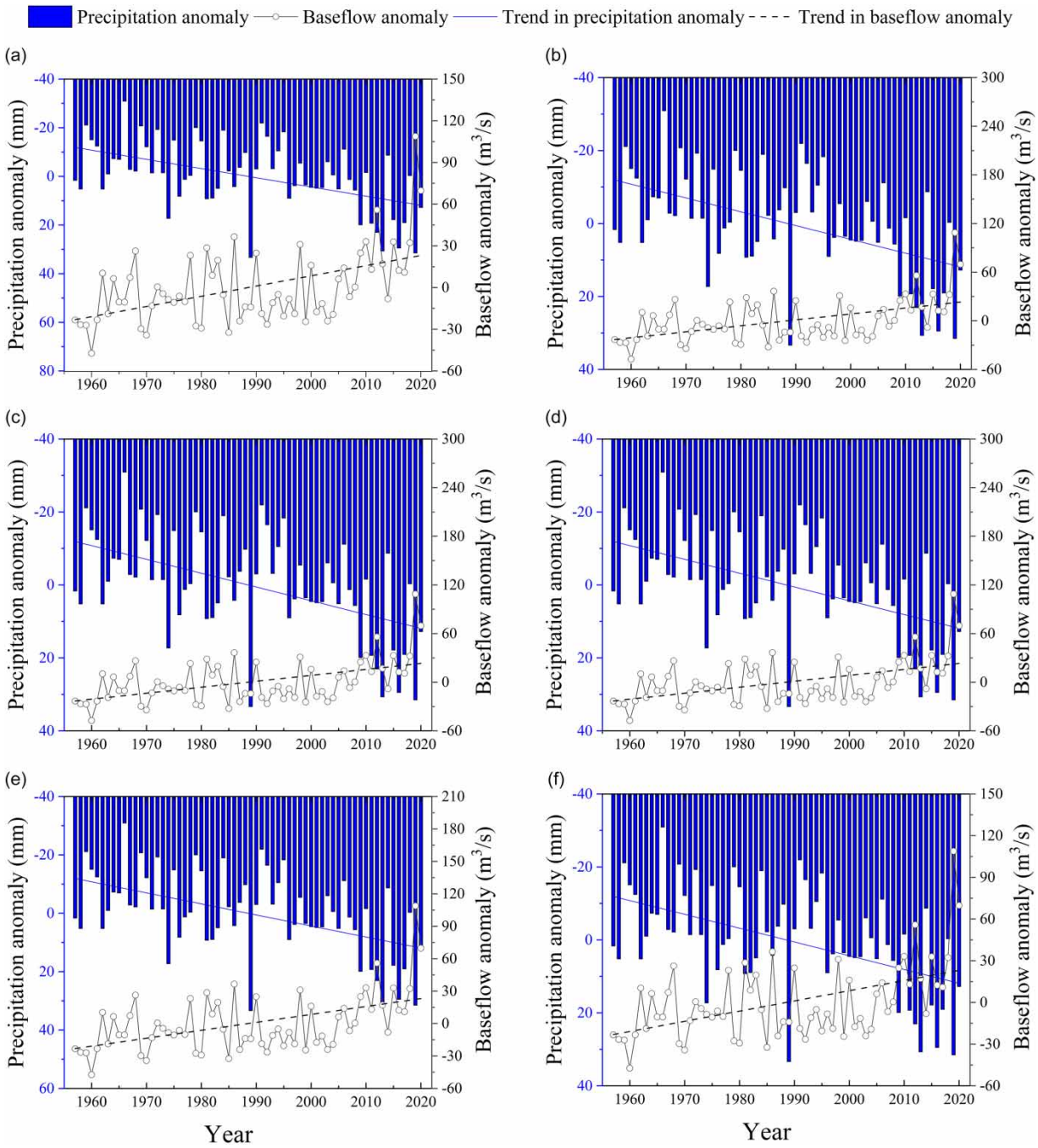

Figure 4 | Temporal variation of baseflow anomaly and BFI in spring (a), summer (b), autumn (c), winter (d), warm months (e), and cold months (f) from 1957 to 2020.

only abrupt points in annual and winter baseflow could be detected by Pettitt's test, and they were found in the years 2000 and 2006. The change of BFI obviously lagged behind that of baseflow, with a delay time of 2 years.

3.3. Intra-annual distribution of baseflow and BFI

Though baseflow and BFI were stable, they still varied throughout the year (Figure 5). It is noteworthy that baseflow and BFI presented distinct intra-annual distribution patterns, namely, that baseflow followed the unimodal distribution, while BFI was in bimodal distribution. Specifically, the baseflow in three consecutive months (July, August, and September) maintained at a

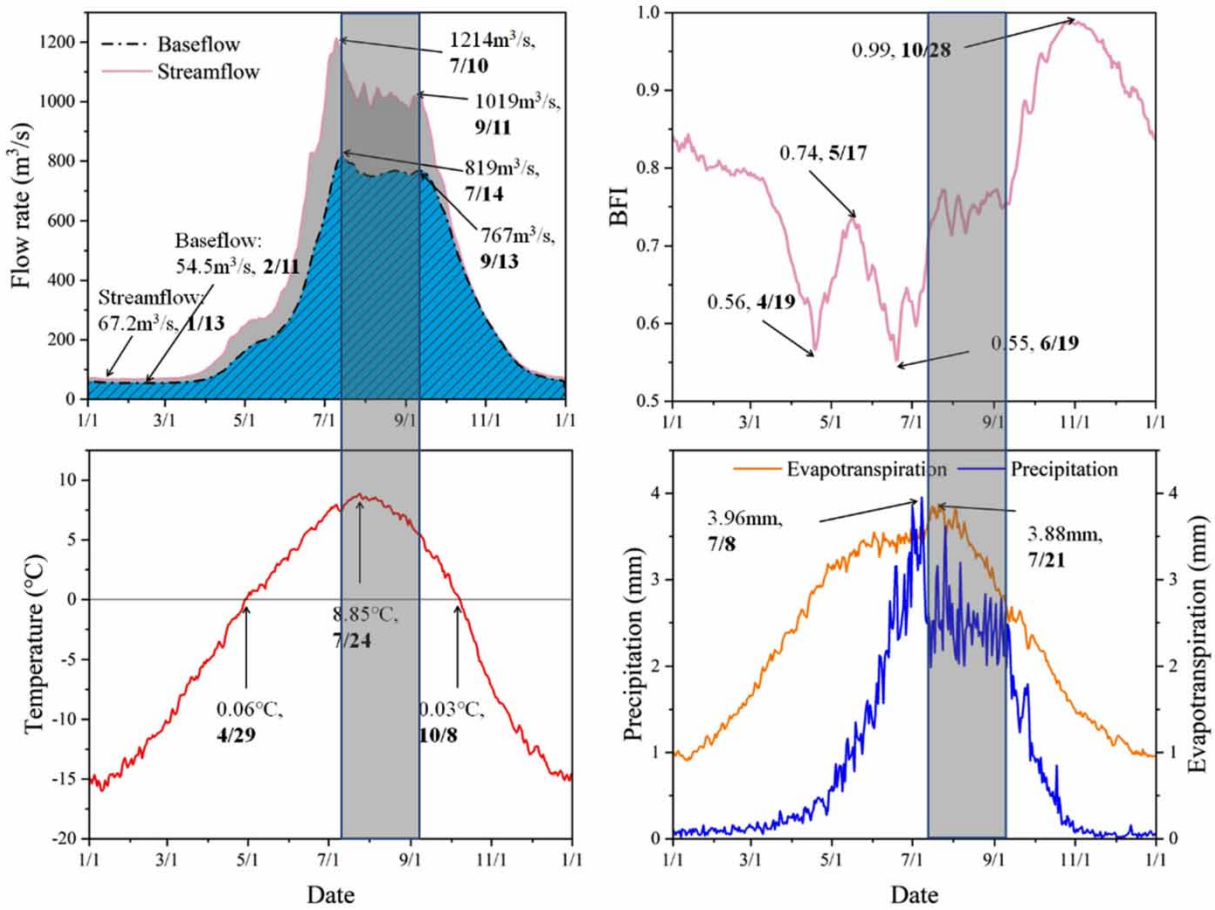

Figure 5 | Intra-annual distribution of streamflow, baseflow, BFI, and climate predictors. The gray interval represents the stationary period of streamflow, baseflow, BFI, and precipitation.

peak level, with the cumulative volume accounting for 60% of annual baseflow. Summer had a much higher baseflow than other seasons, indicating that the baseflow in summertime made a dominant contribution to the total baseflow. In other words, the baseflow was predominantly derived from the warm months, while the baseflow in cold months was significantly lower.

By contrast, BFI in summer and spring were nearly identical and lower than that found in autumn and winter. Compared to the cold months, warm months had a lower BFI. In addition, the BFI had two peaks, one of 0.74 in mid-May and the other of 0.99 in late October. Clearly, the most streamflow in cold months was discharged by groundwater. The mean BFI on April 19 and June 16 reached the two relatively lowest values, 0.56 and 0.55, respectively.

3.4. Temporal variability in meteorological factors

The Mann–Kendall test showed that annual precipitation, evapotranspiration, and temperature consistently exhibited significant upward trends, and the significance of their temperature increase was the greatest (Figures 4 and 6 and Table 1). Throughout the four seasons, temperature increased significantly with time. However, for precipitation and evapotranspiration, only one season had an increasing trend, i.e., spring and winter, respectively. Evidently, we can deduce that the SRYR's climate has become warmer and more humid in the last 64 years.

Pettitt's test demonstrated that precipitation and temperature exhibited significant changes in 1998 and 1997, close to the year of the mutation in baseflow and BFI. Nevertheless, a much earlier breakpoint of evapotranspiration was detected in 1969. It can be inferred from the facts above that precipitation and temperature, not evapotranspiration, played an important role in the long-term evolution of the baseflow in the SRYR.

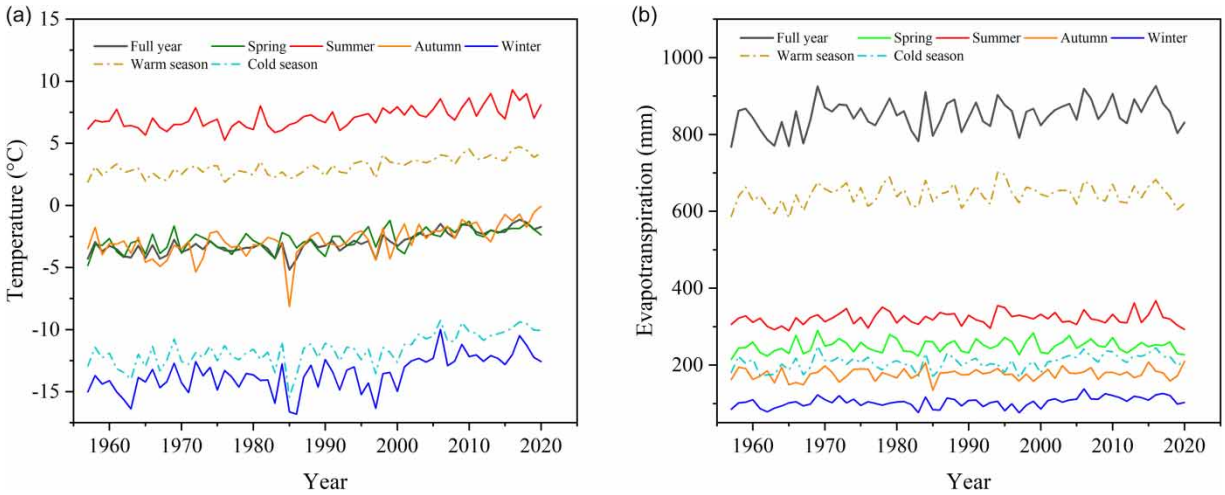

Figure 6 | Temporal variation of annual and seasonal temperature (a) and evapotranspiration (b).

3.5. Correlation of baseflow with meteorological factors

Correlations between baseflow and its corresponding potential climate predictors are presented in Figure 7. Overall, precipitation and temperature had positive relationships with baseflow. Evapotranspiration played a negative role during warm months and a positive role during cold months. The correlation plots showed that precipitation was the dominant factor of the temporal variation of annual baseflow, with a correlation coefficient of 0.84, followed by temperature (0.40) and evapotranspiration (−0.28). Although temperature's effect was not as strong as that of precipitation, it nearly persisted throughout the year. The difference was that precipitation's influence was almost absent in cold months.

Correlations between baseflow and climate parameters varied across seasons and months. All year round, precipitation, temperature, and evapotranspiration played different roles in controlling baseflow. For spring and summer, precipitation made the greatest contribution with correlation coefficients of 0.54 and 0.77, followed by evapotranspiration (−0.38 and −0.58) and then temperature (0.17 and 0.21). For autumn, precipitation and temperature made the top two contributions with correlation coefficients of 0.60 and 0.40, followed by evapotranspiration (−0.13). During winter, temperature made the greatest contribution, with a correlation coefficient of 0.50, followed by evapotranspiration (0.33). However, precipitation had no relationship to the fluctuation of baseflow. Specifically, from October to April of the following year, temperature played a dominant role in driving the increase in baseflow. With April as the exception, the influence of precipitation was almost nonexistent during this period. However, during May to September, precipitation was dominant, followed by evapotranspiration, while temperature's impact was negligible. In other words, during the warm months, precipitation (0.84) made more contribution than evapotranspiration (−0.50) and temperature (0.40). In the cold months, temperature (0.58) made the greatest contribution, compared to evapotranspiration (0.29) and precipitation (0.19).

As seen in Figure 7, there was a response delay in the baseflow caused by meteorological factors, and this response process varied for different periods. There was a significant correlation between baseflow and precipitation in the months of April to September, but their strongest correlation occurred in the second month. This hysteresis of baseflow to precipitation can last several months. For example, the precipitation in September maintained a large influence on the baseflow in the following 10 months. Evapotranspiration exhibited a moderate relationship with baseflow in those same months, and its strong relation was found in the second month, but soon ceased in the third month. Evidently, the delay of baseflow to evapotranspiration lasted only for 1–2 months. Moreover, during January to April and September to October, the strong relationship between temperature and baseflow did not cease until May, and in November, the strong relationship persisted until the second month.

3.6. Contribution of meteorological factors to increase in baseflow

Based on the results of attribution analysis, climate variability contributed the most, with a percentage of 124%; precipitation contributed 86%, temperature 53%, and evapotranspiration −15%. In contrast, the impact of human activity had a small proportion of −24%.

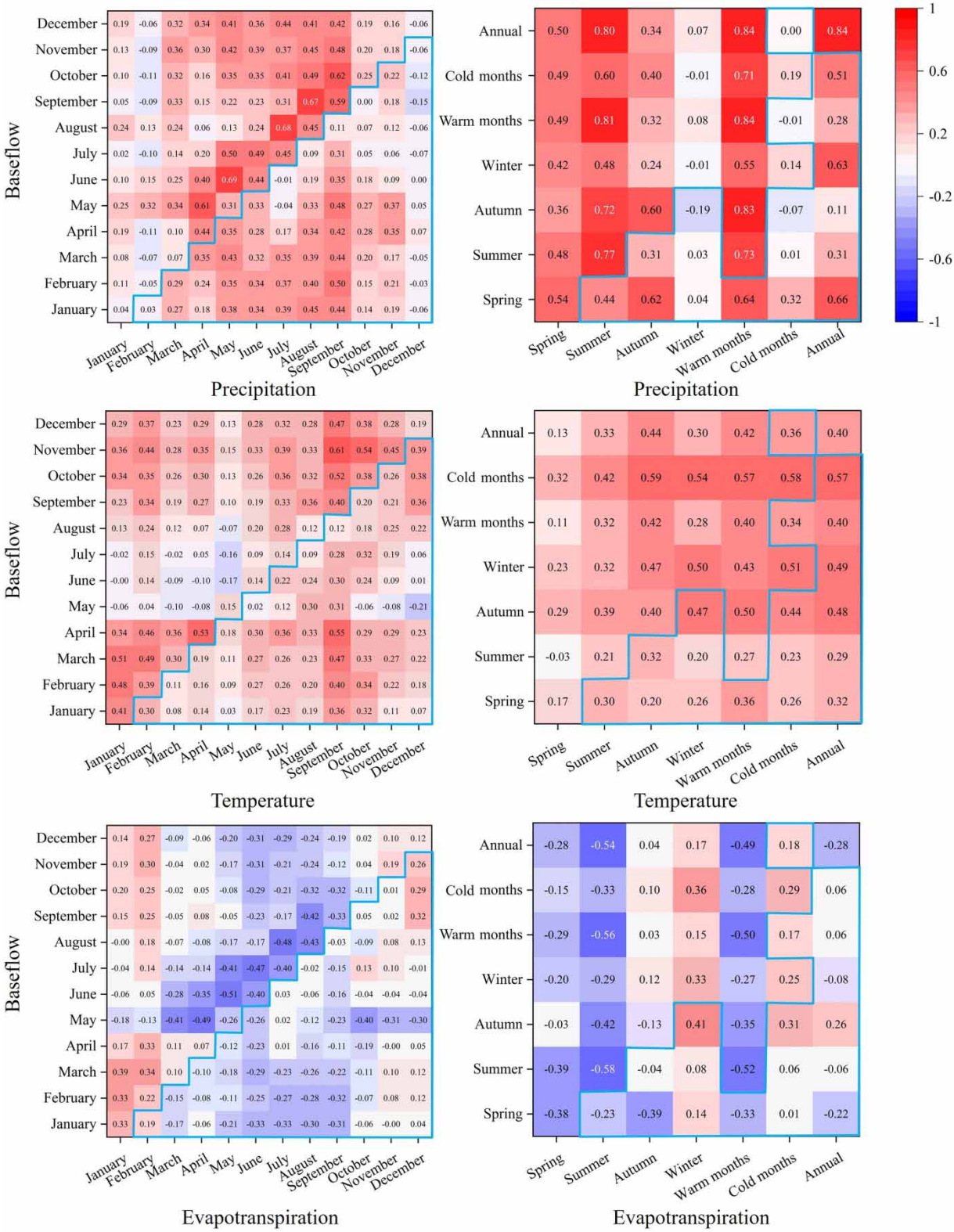

Figure 7 | The correlation of baseflow with climate predictors (precipitation, evapotranspiration, and temperature) at monthly and seasonal scales. The blue boxes indicate the relationship of climate-baseflow between the current and the next year.

4. DISCUSSION

4.1. Critical role of groundwater to streamflow

Groundwater is a vital source of freshwater, and as such, maintaining and enhancing groundwater storage and discharge is central to climate adaptation (Stigter *et al.* 2023; Yin *et al.* 2023a, 2023b, 2023c). Ahiablame *et al.* (2017) pointed out that 60% of streamflow in the Missouri River basin is derived from baseflow. The simulation results from Miller *et al.* (2016) show that 56% of the surface water in the Upper Colorado River Basin originated as baseflow. Aquifers beneath our own study area contain a large amount of solid and liquid groundwater, but its hidden role remains unclear. Compared to the rivers in temperate regions, the SRYR has a much greater proportion of groundwater discharge. Although the streamflow is composed of multiple potential sources, groundwater is the major contributor to runoff generation. Groundwater contributed 62–97% of the monthly mean streamflow, and 75% of the annual mean, indicating a significant role in sustaining the discharge of rivers in the SRYR. Gonzales *et al.* (2009) found a much higher proportion of groundwater in the streamflow in cold regions. For a small catchment in the central part of the Netherlands, approximately 90% of the total runoff comes from groundwater. Our findings corroborated the ideas of Guo *et al.* (2022), who suggested that groundwater contribution is much more important to the glaciated alpine watersheds on the Tibetan Plateau than previously thought. As an underlying system mediator, groundwater can provide relatively stable water sources against extremes, especially in the face of global climate change (Condon *et al.* 2020).

4.2. Lagged effects of baseflow in response to meteorological factors

Baseflow itself is a delayed source, sustaining streamflow in an extended period after precipitation or during periods of drought (Ayers *et al.* 2021). Baseflow is directly associated with precipitation, but there are apparent time lags between the two. Changes in precipitation may drive baseflow discharge by altering the gradient between surface water and groundwater levels. However, the points at which precipitation inputs arrive at surface water and groundwater bodies are vastly different due to their discrepancies of recharging routing. This reflects, in part, the different time scales over which surface water and groundwater operate. This is why there was a delay between baseflow and precipitation in our study. Meanwhile, the hysteresis effect of baseflow on precipitation is diverse across regions. For example, the hysteretic influence of precipitation on baseflow was evident in the US Pacific Northwest and Midwest but was not the case in the remaining areas (Ayers *et al.* 2022). In addition, the precipitation hysteretic effect of baseflow may vary by month. Our results, as shown in Figure 7, also reflected this diversity. The influence of precipitation on baseflow in the SRYR was large during April to September and could be extended for no less than 3 months, but that extension cannot be applied for other months.

Our results also revealed that the delay effect for temperature was similar to that for precipitation, but their influencing mechanisms were completely different. When the daily maximum temperature is greater than 0 °C, the melting of frozen soils or glaciers begin to intensify. However, it will take months for the soils or glaciers to melt, due to slow heat conduction through soils and ice, as well as production and confluence processes. This causes baseflow to lag behind temperature. However, it is noted that the correlation and hysteresis effect of baseflow and temperature were absent from May to August because of the disturbance of precipitation inputs.

The influence mechanism of evapotranspiration on baseflow was similar to that of precipitation, but the impact of evapotranspiration was not significant and lasted for only 1–2 months. This was likely perturbed by the combination of precipitation and temperature.

4.3. Climatic contribution of baseflow variations

A great amount of knowledge has been accumulated on baseflow in the past two decades. Despite this, our understanding of baseflow-generating mechanisms remains rather limited. This limitation is particularly pronounced with alpine areas, where the influence of climate change on baseflow variations is much more intricate (Sun *et al.* 2020).

Precipitation generally plays a dominant role in driving the baseflow variability in unregulated rivers in a variety of climate regions (Miller *et al.* 2016). Globally, precipitation was the most prominent cause for temporal changes in mean runoff for 83% of land grid cells. Here, we have identified that increased precipitation was the most important factor in driving baseflow variations, with a contribution of 86%. This is somewhat smaller than that in other more temperate regions, likely because only some months out of the year experienced precipitation domination during the formation of baseflow. The role of precipitation inputs in the increasing trend of baseflow was lost in the cold months, because during these cold months, the dominant form of precipitation was snow, and the incidence of precipitation recharging baseflow was reduced. It is clear that

precipitation made minimal contributions to baseflow during the winter months, but the long-term mean winter baseflow trend was somewhat influenced by precipitation inputs (Paznekas & Hayashi 2016). Certainly, our results were not always consistent with previous studies. For example, the investigation of Paznekas & Hayashi (2016) showed that precipitation inputs had a strong correlation with the long-term mean winter flow in the Canadian Rockies, reflecting the dominant role of precipitation during wintertime.

A number of researchers have reported that precipitation and evaporation cannot fully explain changes in the baseflow in alpine areas (Ahiablame *et al.* 2017). Temperature is an important predictor in high elevations (Ayers *et al.* 2021). For rivers with melting water from glaciers and permafrost as the main source of recharge, temperature often serves as the primary factor influencing runoff variations (Lin *et al.* 2020). It is worth noting that temperature may also influence baseflow variations by altering the spatiotemporal patterns of precipitation (Yin *et al.* 2023a, 2023b, 2023c), but this is beyond the scope of our study. Many studies have suggested that solid water is the most important source of river water during ablation episodes in the SRYR. Li *et al.* (2020) pointed that the proportion of precipitation for rivers in the SRYR permafrost area was only 20.79%, whereas those of supra-permafrost water and glacier/snow meltwater were 69.54 and 9.67%, respectively. Our study area experienced more rapid changes in temperature than environments at lower elevations (Pepin *et al.* 2015). Our results also show that upward trends in baseflow coincided with an increased temperature. Thus, another reason why baseflow was always increasing is that temperature experienced a marked rising trend. In our study, temperature was a secondary contributor. By comparison, Yi *et al.* (2021) did not agree with our conclusion. They thought that rising temperature was the primary cause. Regardless, temperature played an important role in the generation of baseflow in the SRYR.

In contrast to the direct inputs of precipitation, the influence mechanism and processes of temperature were somewhat complicated and frequently disputed. One universal understanding is that warmer temperatures across cold regions can contribute to increased baseflow, likely from ice/snow melt. On the other hand, increases in temperature can bring about a decline of baseflow, likely through increased evapotranspiration (Murray *et al.* 2023). It can be suggested, then, that temperature can influence baseflow by modifying evapotranspiration rates and the timing of snowmelt runoff. Globally speaking, the increases in temperature were often linked to decreases in baseflow in temperate zones, because warming-induced evapotranspiration was the dominant component. However, that is not the case in alpine regions. In high latitude and altitude regions, baseflow commonly increased with permafrost thaw as a result of warming (Brabets & Walvoord 2009). St. Jacques & Sauchyn (2009) emphasized that increases to baseflow in the Northwest Territories stemmed from permafrost melting. Shi *et al.* (2020) reported that the mean maximum frozen depth of seasonal frozen ground declined by 12.3 cm/10a and the mean active layer of thickness of permafrost increased by 4.2 cm/10a in the SRYR. Of the four seasons, winter had the largest increase rate (0.43 °C per decade), followed by 0.42 °C per decade in autumn. This signifies that temperature increase contributes to earlier melting/later freezing and the extension of the melting period. Clearly, the frozen ground degradation was accelerating, as a strong relationship between baseflow and warming temperature during the cold months had been observed in our study. In winter, there was not a significant trend in precipitation, but a significantly increasing trend in evapotranspiration was found. Thus, the rising baseflow can only be attributed to the melt of glacial snow and permafrost. We therefore speculated that the impact of temperature changes exceeded that of precipitation changes, meaning temperature was the dominant variable in the cold seasons. As is common knowledge, temperature causes changes in the phase states of water. Apart from temperature-induced water inputs, temperature altered groundwater discharges in other indirect ways. Warming-induced permafrost thaw was expected to activate the groundwater flow systems and increase the connectivity between surface water and groundwater, leading to a rise of baseflow. This conclusion was also supported by the strong significant positive correlations between baseflow, the thawing index, and the glacier area change in the study's watersheds (Figure 8). Although some components of rising baseflow can stem from warming-induced glacier and permafrost thawing, it is considered a secondary influencing factor.

By comparison, evapotranspiration was the least important factor to negatively impact baseflow variations, with a small contribution of −11%. That being said, evapotranspiration may sometimes act as a dominant contributor (Smakhtin 2001). For example, as a predictor of baseflow, terrestrial water storage throughout the Arctic experienced a declining trend, and Suzuki *et al.* (2018) largely attributed it to an increase in evapotranspiration driven by rising summer air temperatures.

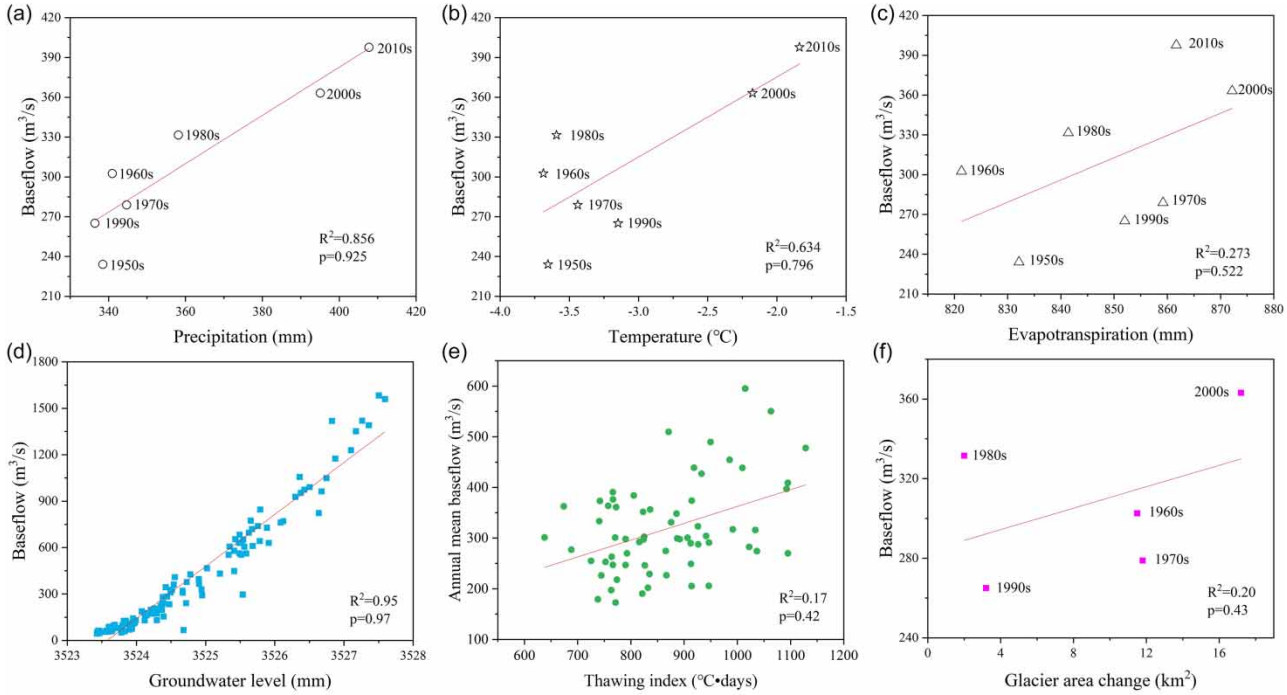

Figure 8 | The relationship between baseflow and precipitation (a), temperature (b), evapotranspiration (c), groundwater level (d), thawing index (e), and glacier area change (f).

4.4. Possible role of anthropogenic activities

Perhaps the greatest obstacle in assessing baseflow response to climate change is the confounding factor of concurrent anthropogenic activity. Anthropogenic activities in the SRYR included the implementation of ECPs, water withdrawal for domestic purposes, and grazing-induced land cover change. However, this source area was recently a depopulated zone because of poverty and harsh environments. More and more residents moved away from this area after 2000 when massive ecological migrations were initiated. Considering that the population in headwaters was sparse, the influences of water withdrawal and grazing were approaching zero and can consequently be neglected in the attribution of baseflow. Therefore, the ECPs may represent much of the human activity in this area.

The ECPs in this area, including Wetland Protection Program and Desertification Land Control Program, greatly changed land use and land cover (LULC), producing significant ecological effects. The evidence that vegetation coverage is continuously increasing in the SRYR in recent years has been widely reported. According to the Statistical Bulletin of National Economic and Social Development of Yushu Prefecture, more than 130 million sporadic plants and 200,000 hectares of grasslands have been developed. Rodents have been wiped out in more than 5,000,000 hectares since the implementation of ECPs. As of now, water conservation has increased by more than 6% annually, and grassland coverage and grass production have risen by more than 11 and 30%, respectively, compared to 10 years ago. Certainly, vegetation cover could be an integrated index (Tan *et al.* 2020), and its development was prompted not only by the implementation of ECPs but also by the rising temperatures, precipitation, and atmospheric CO_2 (Zhang *et al.* 2022). The LULC change reflected by these statistics may lead to the alteration of the water cycle and water retention capacity, thus directly affecting the baseflow-generating processes. Our findings show that the ECPs essentially representing the impact of human activities can explain −24% of the increasing baseflow trends, indicating a negative relationship between baseflow and ECPs. This is somewhat consistent with results from other studies (Brown *et al.* 2005). A large number of studies on the impact of land cover change on baseflow revealed a statistically significant negative association between changes in baseflow and basin vegetation (Tan *et al.* 2020). Essentially, evapotranspiration was limited by water availability (Babst *et al.* 2019). The additional grasslands may improve water retention by trapping precipitation in the vegetation canopy, litter, and soil layers, resulting in a persistent increase in

the actual evaporation rate (Trancoso *et al.* 2017). Soil drying would be exacerbated, ultimately leading to a reduction in baseflow. Additional vegetation cover may improve the transpiration rate, thereby greatly consuming shallow groundwater (Condon *et al.* 2020). Thus, this negative relationship between catchment vegetation cover and baseflow volume may be due to greater interception and evapotranspiration rates associated with vegetation cover.

5. CONCLUSIONS AND FUTURE PROSPECTS

5.1. Conclusions

The main purpose of this study was to investigate dynamic characteristics of baseflow variations and identify possible climatic and anthropogenic drivers across the SRYR. Sixty-four years of hydrological records were gathered from the Zhimenda gauging station at the catchment outlet to investigate the changes in annual and monthly baseflow and BFI across the whole watershed. Statistical monotonic trends and corresponding trend slopes were determined using the Mann–Kendall test and Sen's Slope test, and breakpoints were detected using Pettitt's test. Correlation analysis and the elasticity approach were carried out to study the contributions of climate change and human activity to changes in baseflow.

The Eckhardt method was assessed to be the most suitable approach in the SRYR. Annual and seasonal trends in baseflow and temperature were consistently increasing, which was not the case for precipitation and evapotranspiration; annual precipitation and evapotranspiration had a rising trend, but only springtime precipitation and wintertime evapotranspiration increased. In addition, time lags between baseflow and climate parameters were found, and the hysteretic effects varied for different climate parameters and months.

We found that the roles of precipitation, temperature, and evapotranspiration were distinct in spring, summer, autumn, and winter. Of the three climate predictors, precipitation was the most critical driver in contributing to the change in baseflow, followed by temperature, and then evapotranspiration. The contributions of precipitation, temperature, and evapotranspiration on baseflow were 86, 53, and −15%, respectively. However, across the four seasons, the three predictors played different roles in influencing baseflow. Precipitation made the greatest contribution in spring and summer, followed by evapotranspiration and temperature. In autumn, precipitation and temperature made the greatest contributions, followed by evapotranspiration. In winter, temperature made the greatest contribution, followed by evapotranspiration. The contribution of precipitation was so minute that it can be overlooked. On a monthly scale, from October to April of the following year, temperature played a dominant role in the evolution of baseflow, while the effect of precipitation was almost absent (except in April). During the period from May to September, precipitation was dominant, followed by evapotranspiration, while the impact of temperature was negligible. In addition, ECP-induced vegetation cover greening made a negative contribution of −24% to the increase in baseflow.

All in all, the glacier/permafrost melting water and snowmelt associated with increasing temperature, in addition to the increasing precipitation inputs, drove the increase in groundwater discharge, albeit under the negative influence of evapotranspiration and ECP implementations. The variation of baseflow was the result of the combined effect of the aforementioned factors. Clearly, the increased temperature superimposed changes upon the precipitation effect. The hydrologic effect of precipitation could be exacerbated by temperature change in the future.

5.2. Future prospects

Although our results highlighted temporal patterns in baseflow and its attributions, the spatial variability was less seriously considered. The baseflow-generating mechanisms vary with elevation, and patterns of baseflow variability may be of small difference across the source region. In the future, a distributed hydrological model coupling the melted ground and glacial snow should be constructed to investigate the spatial pattern of baseflow.

Furthermore, with the steady progress of the pilot program for the Sanjiangyuan National Park and the comprehensive implementation of the Qinghai–Tibet Plateau Ecological Protection Law, the vegetation in the SRYR will experience long-term positive development. This will lead to a further enhancement of water source conservation capacity, profoundly affecting the future trends in baseflow changes. Moreover, according to the Climate Change 2022: Impacts, Adaptation and Vulnerability released by IPCC, under the backdrop of climate change, future runoff variations are uncertain and complexities are heightened, emphasizing the more pronounced role of baseflow in stabilizing runoff. Hence, accurate baseflow prediction is crucial, necessitating comprehensive consideration of vegetation cover and the impacts of climate change.

AUTHOR CONTRIBUTIONS

GW contributed to the methodology, formal analysis, writing – original draft, writing – review & editing, and funding acquisition. JZ contributed to the methodology, conceptualization, and supervision. YL contributed to the data curation and validation. YL and MY contributed to the investigation and validation. HR contributed to the visualization.

ACKNOWLEDGEMENTS

This research was jointly funded by the National Key Research and Development Programs of China (No. 2022YFC3201700), the National Natural Science Foundation of China (No. 52009006), and the Fundamental Research Funds for Central Public Welfare Research Institutes (No. CKSF2023315/TB). We also acknowledge the Qinghai Hydrology and Water Resources Survey Center for data support.

DATA AVAILABILITY STATEMENT

All relevant data are included in the paper or its Supplementary Information.

CONFLICT OF INTEREST

The authors declare there is no conflict.

REFERENCES

Ahiablame, L., Sheshukov, A. Y., Rahmani, V. & Moriasi, D. 2017 Annual baseflow variations as influenced by climate variability and agricultural land use change in the Missouri River Basin. *J. Hydrol.* **551**, 188–202.

Ayers, J. R., Villarini, G., Schilling, K. & Jones, C. 2021 On the statistical attribution of changes in monthly baseflow across the U.S. Midwest. *J. Hydrol.* **592**, 125551.

Ayers, J. R., Villarini, G., Schilling, K., Jones, C., Brookfield, A., Zipper, S. C. & Farmer, W. H. 2022 The role of climate in monthly baseflow changes across the continental United States. *J. Hydrol. Eng.* **27**, 04022006.

Babst, F., Bouriaud, O., Poulter, B., Trouet, V., Girardin, M. P. & Frank, D. C. 2019 Twentieth century redistribution in climatic drivers of global tree growth. *Sci. Adv.* **5**, eaat4313.

Brabets, T. P. & Walvoord, M. A. 2009 Trends in streamflow in the Yukon River Basin from 1944 to 2005 and the influence of the Pacific Decadal Oscillation. *J. Hydrol.* **371**, 108–119.

Brown, A. E., Zhang, L., McMahon, T. A., Western, A. W. & Vertessy, R. A. 2005 A review of paired catchment studies for determining changes in water yield resulting from alterations in vegetation. *J. Hydrol.* **310**, 28–61.

Brutsaert, W. 2008 Long-term groundwater storage trends estimated from streamflow records: Climatic perspective. *Water Resour. Res.* **44**, W02409.

Chen, H. & Teegavarapu, R. S. V. 2021 Spatial and temporal variabilities in baseflow characteristics across the continental USA. *Theor. Appl. Climatol.* **143**, 1615–1629.

Cheng, L., Zhang, L., Chiew, F. H. S., Canadell, J. G., Zhao, F., Wang, Y., Hu, X. & Lin, K. 2017 Quantifying the impacts of vegetation changes on catchment storage-discharge dynamics using paired-catchment data. *Water Resour. Res.* **53**, 5963–5979.

Condon, L. E., Atchley, A. L. & Maxwell, R. M. 2020 Evapotranspiration depletes groundwater under warming over the contiguous United States. *Nat. Commun.* **11**, 873.

Cui, T., Li, Y., Yang, L., Nan, Y., Li, K., Tudaji, M., Hu, H., Long, D., Shahid, M., Mubeen, A., He, Z., Yong, B., Lu, H., Li, C., Ni, G., Hu, C. & Tian, F. 2023 Non-monotonic changes in Asian Water Towers' streamflow at increasing warming levels. *Nat. Commun.* **14**, 1176.

Duan, L., Man, X., Kurylyk, B. L. & Cai, T. 2017 Increasing winter baseflow in response to permafrost thaw and precipitation regime shifts in Northeastern China. *Water* **9**, 25.

Eckhardt, K. 2005 How to construct recursive digital filters for baseflow separation. *Hydrol. Process.* **19**, 507–515.

Ficklin, D. L., Robeson, S. M. & Knouft, J. H. 2016 Impacts of recent climate change on trends in baseflow and stormflow in United States watersheds. *Geophys. Res. Lett.* **43**, 5079–5088.

Gnann, S. J., Woods, R. A. & Howden, N. J. K. 2019 Is there a baseflow Budyko curve? *Water Resour. Res.* **55**, 2838–2855.

Gonzales, A. L., Nonner, J., Heijkers, J. & Uhlenbrook, S. 2009 Comparison of different base flow separation methods in a lowland catchment. *Hydrol. Earth Syst. Sci.* **13**, 2055–2068.

Guo, X., Feng, Q., Yin, Z., Si, J., Xi, H. & Zhao, Y. 2022 Critical role of groundwater discharge in sustaining streamflow in a glaciated alpine watershed, northeastern Tibetan Plateau. *Sci. Total Environ.* **822**, 153578.

Kayitesi, N. M., Guzha, A. C. & Mariethoz, G. 2022 Impacts of land use land cover change and climate change on river hydro-morphology – A review of research studies in tropical regions. *J. Hydrol.* **615**, 128702.

Li, Z., Li, Z., Feng, Q., Zhang, B., Gui, J., Xue, J. & Gao, W. 2020 Runoff dominated by supra-permafrost water in the source region of the Yangtze river using environmental isotopes. *J. Hydrol.* **582**, 124506.

Li, H., Wang, W., Fu, J. & Wei, J. 2023a Spatiotemporal heterogeneity and attributions of streamflow and baseflow changes across the headstreams of the Tarim River Basin, Northwest China. *Sci. Total Environ.* **856**, 159230.

Li, Z., Liu, M., Li, Z., Feng, Q., Song, L., Xu, B., Liu, X. & Gui, J. 2023b Where does the runoff come from in dry season in the source region of the Yangtze River? *Agric. For. Meteorol.* **330**, 109314.

Lin, L., Gao, M., Liu, J., Wang, J., Wang, S., Chen, X. & Liu, H. 2020 Understanding the effects of climate warming on streamflow and active groundwater storage in an alpine catchment: The upper Lhasa River. *Hydrol. Earth Syst. Sci.* **24** (3), 1145–1157.

Liu, J., Chen, J., Xu, J., Lin, Y., Yuan, Z. & Zhou, M. 2019 Attribution of runoff variation in the headwaters of the Yangtze River based on the Budyko hypothesis. *Int. J. Environ. Res. Public Health.* **16**, 2506.

Lott, D. A. & Stewart, M. T. 2016 Base flow separation: A comparison of analytical and mass balance methods. *J. Hydrol.* **535**, 525–533.

Lucas, M. C., Kublik, N., Rodrigues, D. B. B., Meira Neto, A. A., Almagro, A., Melo, D. D. C. D., Zipper, S. C. & Oliveira, P. T. S. 2020 Significant baseflow reduction in the Sao Francisco River Basin. *Water* **13**, 2.

Luo, K. 2022 Contribution of ecological conservation programs and climate change to hydrological regime change in the source region of the Yangtze River in China. *Reg. Environ. Change* **22**, 10.

Miller, M. P., Buto, S. G., Susong, D. D. & Rumsey, C. A. 2016 The importance of base flow in sustaining surface water flow in the Upper Colorado River Basin. *Water Resour. Res.* **52**, 3547–3562.

Mukherjee, A., Bhanja, S. N. & Wada, Y. 2018 Groundwater depletion causing reduction of baseflow triggering Ganges river summer drying. *Sci. Rep.* **8**, 12049.

Murray, J., Ayers, J. & Brookfield, A. 2023 The impact of climate change on monthly baseflow trends across Canada. *J. Hydrol.* **618**, 129254.

Paznekas, A. & Hayashi, M. 2016 Groundwater contribution to winter streamflow in the Canadian Rockies. *Can. Water Resour. J.* **41**, 484–499.

Pepin, N., Bradley, R., Diaz, H., Baraer, M. & Caceres, E. 2015 Elevation-dependent warming in mountain regions of the world. *Nat. Clim. Change* **5**, 424–430.

Pettyjohn, W. A. & Henning, R. J. 1979 *Preliminary Estimate of Regional Effective Ground-Water Recharge Rates, Related Streamflow and Water Quality in Ohio*. Water Resource Center, Columbus, OH.

Rounce, D. R., Hock, R., Maussion, F., Hugonnet, R., Kochtitzky, W., Huss, M., Berthier, E., Brinkerhoff, D., Compagno, L., Copland, L., Farinotti, D., Menounos, B. & McNabb, R. W. 2023 Global glacier change in the 21st century: Every increase in temperature matters. *Science* **379**, 78–83.

Scanlon, B. R., Fakhreddine, S., Rateb, A., De Graaf, I., Famiglietti, J., Gleeson, T., Grafton, R. Q., Jobbagy, E., Kebede, S., Kolusu, S. R., Konikow, L. F., Long, D., Mekonnen, M., Schmied, H. M., Mukherjee, A., MacDonald, A., Reedy, R. C., Shamsudduha, M., Simmons, C. T., Sun, A., Taylor, R. G., Villholth, K. G., Vörösmarty, C. J. & Zheng, C. 2023 Global water resources and the role of groundwater in a resilient water future. *Nat. Rev. Earth. Environ.* **4**, 87–101.

Segura, C., Noone, D., Warren, D., Jones, J. A., Tenny, J. & Ganio, L. M. 2019 Climate, landforms, and geology affect baseflow sources in a mountain catchment. *Water Resour. Res.* **55**, 5238–5254.

Shi, R., Yang, H. & Yang, D. 2020 Spatiotemporal variations in frozen ground and their impacts on hydrological components in the source region of the Yangtze River. *J. Hydrol.* **590**, 125237.

Sloto, R. A. & Crouse, M. 1996 *HYSEP: A Computer Program for Streamflow Hydrograph Separation and Analysis (Water-Resources Investigations Report)*. U.S. Geological Survey.

Smakhtin, V. U. 2001 Low flow hydrology: A review. *J. Hydrol.* **240**, 147–186.

Stigter, T. Y., Miller, J., Chen, J. & Re, V. 2023 Groundwater and climate change: Threats and opportunities. *Hydrogeol. J.* **31**, 7–10.

St. Jacques, J. & Sauchyn, D. J. 2009 Increasing winter baseflow and mean annual streamflow from possible permafrost thawing in the Northwest Territories, Canada. *Geophys. Res. Lett.* **36**, L01401.

Sun, A., Yu, Z., Zhou, J., Acharya, K., Ju, Q., Xing, R., Huang, D. & Wen, L. 2020 Quantified hydrological responses to permafrost degradation in the headwaters of the Yellow River (HWYR) in High Asia. *Sci. Total Environ.* **712**, 135632.

Suzuki, K., Matsuo, K., Yamazaki, D., Ichii, K., Iijima, Y., Papa, F., Yanagi, Y. & Hiyama, T. 2018 Hydrological variability and changes in the Arctic circumpolar tundra and the three largest pan-Arctic River basins from 2002 to 2016. *Remote Sens.* **10**, 402.

Tan, X., Liu, B. & Tan, X. 2020 Global changes in baseflow under the impacts of changing climate and vegetation. *Water Resour. Res.* **56**, e2020WR027349.

Tetzlaff, D. & Soulsby, C. 2008 Sources of baseflow in larger catchments – Using tracers to develop a holistic understanding of runoff generation. *J. Hydrol.* **359**, 287–302.

Trancoso, R., Larsen, J. R., McVicar, T. R., Phinn, S. R. & McAlpine, C. A. 2017 CO_2-vegetation feedbacks and other climate changes implicated in reducing base flow. *Geophys. Res. Lett.* **44**, 2310–2318.

Wahl, K. L. & Wahl, T. L. 1995 Determining the flow of Comal Springs at New Braunfels, Texas. In: *Proceedings of Texas Water*, San Antonio, TX, pp. 77–86.

Woo, M., Arain, M. A., Mollinga, M. & Yi, S. 2004 A two-directional freeze and thaw algorithm for hydrologic and land surface modelling. *Geophys. Res. Lett.* **31**, L12501.

Xie, J., Liu, X., Wang, K., Yang, T., Liang, K. & Liu, C. 2020 Evaluation of typical methods for baseflow separation in the contiguous United States. *J. Hydrol.* **583**, 124628.

Yi, W., Feng, Y., Liang, S., Kuang, X., Yan, D. & Wan, L. 2021 Increasing annual streamflow and groundwater storage in response to climate warming in the Yangtze River source region. *Environ. Res. Lett.* **16**, 084011.

Yin, J., Gentine, P., Slater, L., Gu, L., Pokhrel, Y., Hanasaki, N., Guo, S., Xiong, L. & Schlenker, W. 2023a Future socio-ecosystem productivity threatened by compound drought–heatwave events. *Nat. Sustain.* **6**, 259–272.

Yin, J., Guo, S., Wang, J., Chen, J., Zhang, Q., Ge, L., Yang, Y., Tian, J., Xiong, L. & Zhang, Y. 2023b Thermodynamic driving mechanisms for the formation of global precipitation extremes and ecohydrological effects. *Sci. China Earth Sci.* **66**, 92–110.

Yin, J., Slater, L. J., Khouakhi, A., Yu, L., Liu, P., Li, F., Pokhrel, Y. & Gentine, P. 2023c GTWS-MLrec: Global terrestrial water storage reconstruction by machine learning from 1940 to present. *Earth Syst. Sci. Data.* **15**, 5597–5615.

Zhang, Y., Gentine, P., Luo, X., Lian, X., Liu, Y., Zhou, S., Michalak, A. M., Sun, W., Fisher, J. B., Piao, S. & Keenan, T. F. 2022 Increasing sensitivity of dryland vegetation greenness to precipitation due to rising atmospheric CO_2. *Nat. Commun.* **13**, 1–9.

Zomlot, Z., Verbeiren, B., Huysmans, M. & Batelaan, O. 2015 Spatial distribution of groundwater recharge and base flow: Assessment of controlling factors. *J. Hydrol. Reg. Stud.* **4**, 349–368.

First received 23 November 2023; accepted in revised form 22 January 2024. Available online 29 February 2024